Frequency Content Effect on the Efficiency of Wavelet and Hilbert-Huang Transforms for Health Monitoring

L.A. Montejo, L.R. Velazquez & R.I. Ramirez
University of Puerto Rico at Mayaguez, Mayaguez, PR

Z. Jiang & R.E. Christenson
University of Connecticut, Storrs, CT

15 WCEE
LISBOA 2012

SUMMARY:
A simply supported single-span steel bridge model was used to evaluate the capability of Wavelet and Hilbert-Huang Transforms for system identification of structures with time changing dynamic properties. The bridge was excited using an electro-dynamic shaker located near the bridge mid-span. The frequency band of the induced noise excitation was controlled to examine its effect on the efficiency of the signal processing methodologies. In order to introduce a discontinuity and a frequency shift in the response of the bridge, mass was added (or removed) during each test. The results obtained show that if both, high and low frequencies analyzes are used, one can get a more clear idea of the changes undergone by the structure. It was also noticed that increasing the high frequency content of the excitation has a detrimental effect in the efficiency of the signal processing techniques evaluated.

Keywords: system identification, dynamic testing, damage detection, empirical mode decomposition

1. INTRODUCTION

This paper presents an experimental evaluation of Wavelet and Hilbert-Huang approaches for identification of natural frequencies changes in systems subjected to random excitations, special emphasis is placed on the effect of different levels of frequency content in the load excitation. First, Wavelet and Hilbert Huang transforms are briefly introduced and their parameters are calibrated using a toy signal with frequency variations similar to the observed on the experimental tests. Once the parameters of both transforms are calibrated using the simplified artificially generated signal, the accelerations recorded during the experimental tests are examined.

2. HILBERT – HUANG TRANSFORM (HHT)

The Hilbert Transform (HT) is perhaps the easiest ways to compute the instant frequency and instant amplitude of a mono-component signal. The HT of a function *x(t)* is defined as:

$$H[x(t)] = \frac{1}{\pi}\int_{-\infty}^{+\infty}\frac{x(\tau)}{t-\tau}d\tau \tag{2.1}$$

With the HT, the Gabor analytic signal *z(t)* (Gabor 1946) of the function *x(t)* can be generated as:

$$z(t) = x(t) + iy(t) = x(t) + iH[x(t)] = a(t)e^{i\theta(t)} \tag{2.2}$$

where:

$$a(t) = \sqrt{x^2 + y^2} \quad \text{and} \quad \theta(t) = \arctan\left(\frac{y}{x}\right) \tag{2.3}$$

The analytic signal decomposes a signal in their instant amplitude *a(t)* and instant phase *θ(t)* component, the instant frequency (IF) is defined as the time derivative of the phase:

$$IF(t) = \frac{1}{2\pi}\frac{d}{dt}\theta(t) \tag{2.4}$$

If applied to a multi-component signal, the HT will still identify only one instant frequency that represent the average of the frequencies occurring in the signal. Multi-component signals need to be first decomposed into its mono-components constituents using methodologies like the Empirical Mode Decomposition (Huang et al. 1998), the Hilbert Vibration Decomposition (Feldman 2006), the Synchrosqueezed Transform (Dabuchies et al. 2011) or band-pass filtering. In this work the Empirical Mode Decomposition (EMD) algorithm is employed, which is perhaps the most popular of these methodologies. The process of applying the EMD and then the HT individually to the mono-components (or Intrinsic Mode Functions IMFs) is known as the Hilbert-Huang Transform (HHT). The EMD is an iterative sifting algorithm where the signal is decomposed into IMFs and a residue. These IMFs are defined so as to ensure that they have well-behaved HTs and conform to a narrowband condition. The EMD was implemented in this work by means of the algorithm provided by Rilling et al. (2003). In this algorithm the stopping criteria for sifting is aimed at guaranteeing globally small fluctuations in the mean while taking into account locally large excursions. The toy signal displayed in Fig. 1 was used to calibrate the algorithm parameters; the signal was generated with similar frequency content and variations to the observed in the experimental tests. Sampling frequency was 1024 Hz and total duration was 40 seconds, the first 20 seconds the signal is composed of 2 sinusoidals of 22 Hz and 24.5 Hz, after 20 seconds the frequencies are shifted to 21Hz and 24 Hz. For discernibility reasons, Fig. 1 shows only the portion of the signal between times 19 and 21 seconds, notice that no discontinuity is evident to the eye at 20 seconds. Fig. 2 shows the IMFS extracted via EMD using stopping parameters [θ1 θ1 α] = [0.05 0.5 0.05]x10^-4 (Rilling et al. 2003). When the instant frequencies for each IMF are calculated via HT the resulting values exhibit an oscillatory behavior around the target frequencies (Fig. 3). To deal with this problem we proceed to smooth the calculated IFs by averaging over a time window of 2 seconds, the result is displayed in Fig. 4. It is seen that the variations of the frequency content over time are successfully identified.

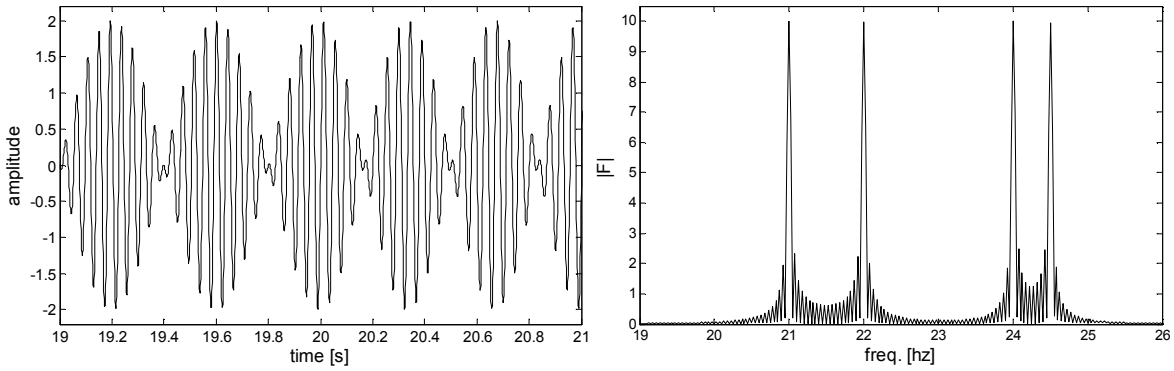

Figure 1. Simulated signals on the time (left) and frequency (right) domains.

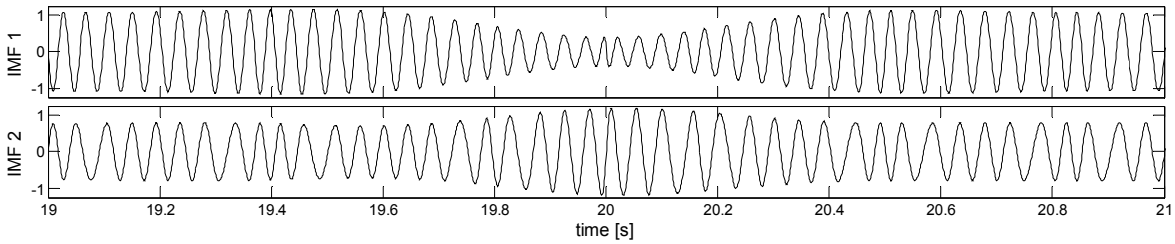

Figure 2. Extracted modal responses via empirical mode decomposition for the signal without noise

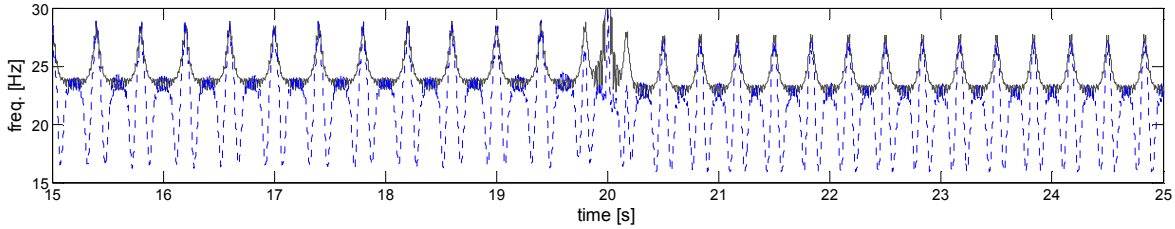

Figure 3. Instant frequency for each modal component via HT

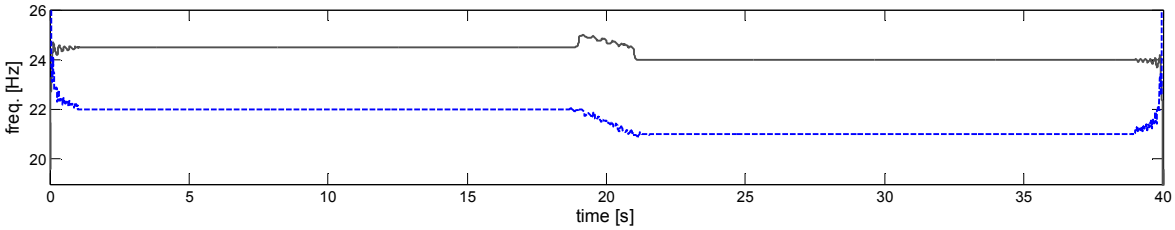

Figure 4. Instant frequency smoothed (averaged) using a 2 seconds window

3. WAVELET TRANSFORM

The Continuous Wavelet Transform (CWT) of a signal *x(t)* is defined as the convolution of the signal and scaled, shifted versions of the mother wavelet *ψ(t)*:

$$W(a,b) = \frac{1}{\sqrt{a}} \int_{-\infty}^{+\infty} x(t) \psi\left(\frac{t-b}{a}\right) dt \tag{3.1}$$

The wavelet coefficients *W(a,b)* contain information about the function *x(t)* at the scale *a* (which can be related with frequency) and around the time position *b*. A modified version of Complex Morlet Wavelet (Grossman and Morlet 1990, Yan and Miyamoto 2006) is used in the applications presented in this article:

$$\psi(t) = \frac{1}{\sqrt{\pi f_b}} e^{i 2\pi f_c t} e^{-t^2 / f_b} \tag{3.2}$$

where f_b is a bandwidth parameter that controls the shape of the mother wavelet and f_c is the central frequency of the mother wavelet. Using the Heisenberg uncertainty principle it can be shown that the time and frequency resolutions for this wavelet at a frequency f_i are given by:

$$\Delta t_i = \frac{f_c}{f_i}\frac{\sqrt{f_b}}{2} \quad \text{and} \quad \Delta f_i = \frac{f_i}{f_c}\frac{1}{2\pi\sqrt{f_b}} \tag{3.3}$$

The wavelet coefficients *W(a,b)* resulting from applying the CWT along with the modified Complex Morlet wavelet to the toy signal are shown in its absolute values in the Wavelet Maps displayed in Fig. 5. The wavelet analysis is performed at the low (Fig. 5 bottom) and high frequency (Fig. 5 top) ranges. The low frequency analysis was performed using parameters $f_b=10$ and $f_c=24$, the critical resolution values are then $\Delta t=1.807$ *s* ($f_i=21$ *Hz*) and $\Delta f=0.0514$ *Hz* ($f_i=24.5$ *Hz*). The high frequency analysis was performed using parameters $f_b=1$ and $f_c=1$, the critical resolution values are then $\Delta t= 0.0238$ *s* ($f_i=21$ *Hz*) and $\Delta f= 3.8993$ *Hz* ($f_i=24.5$ *Hz*). For the high frequency analysis the time axis was limited to the range 19-21 seconds so that the discontinuity is observable. It can be seen that through the analysis at both frequency ranges not only the change in the frequencies of vibration can be examined but also the exact time instant where the change took place.

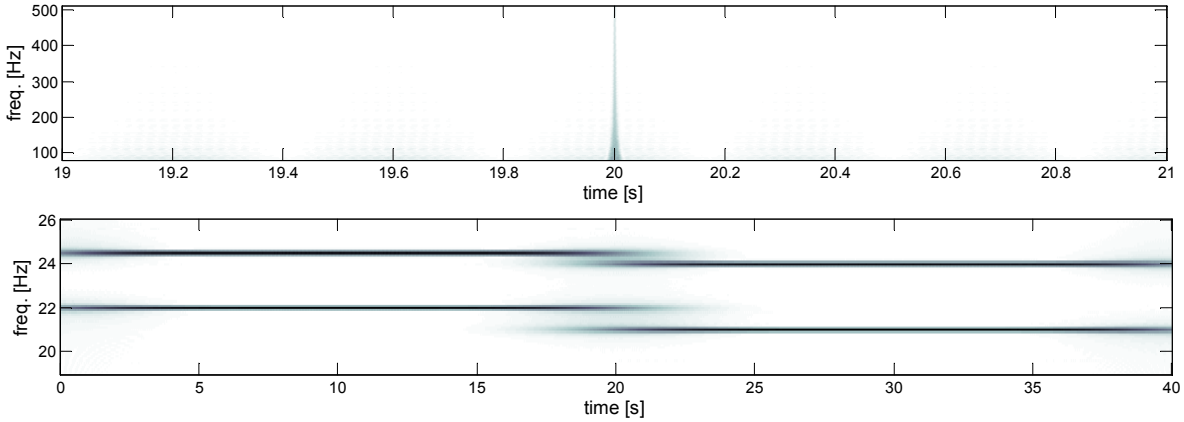

Figure 5. High (top) and low (bottom) frequency wavelet analysis

4. EXPERIMENTAL TESTS

A simply supported single-span bridge model (Fig. 6) was used to evaluate the behavior of the signal-processing based identification methodologies using experimental vibrational data. The bridge was excited with different vertical noise vibrations using an electro-dynamic shaker located near the bridge mid-span. The frequency band of the induced noise vibrations was controlled to examine the effect of the excitation frequency content on the efficiency of the SP methodologies. Five different excitations were imposed ranging from frequency contents between [0-30] Hz to [0-100] Hz (Fig. 7). In order to induce a discontinuity and a frequency shift in the response of the bridge, mass was added or removed during each test through a 44.5lb bucket connected to the laboratory crane. The induced load and bridge vibrations were monitored through 7 piezoelectric accelerometers distributed along the bridge. Fig. 8 shows the recorded accelerations at mid-span of the bridge for all the cases analyzed. It is seen that while identification of the discontinuity produced by the change in mass is obvious in the "added mass" cases, for the "removed mass" cases such identification is not evident.

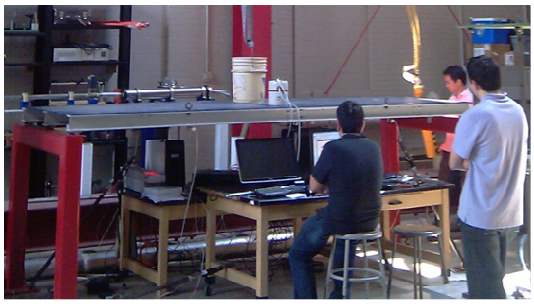

Figure 6. Single span bridge model

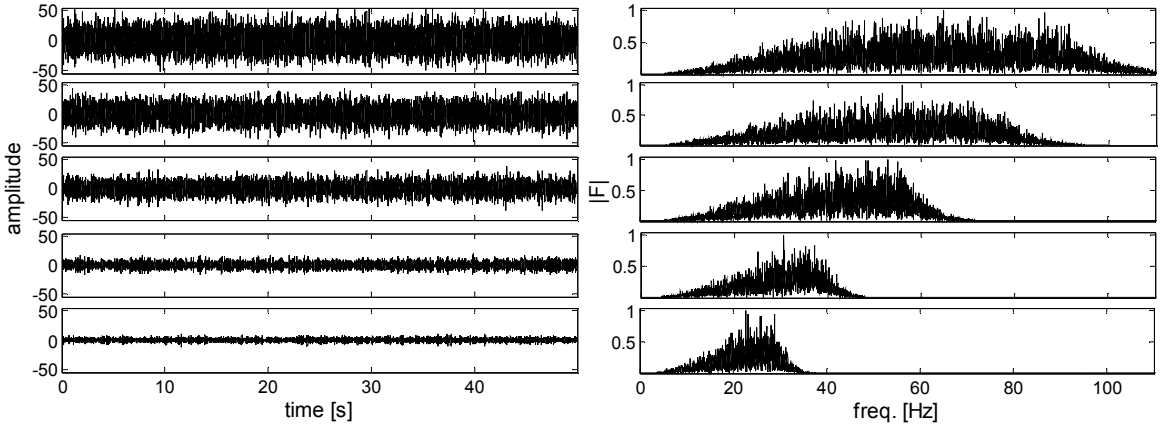

Figure 7. Measured excitation loads in the time (left) and frequency (right) domains.

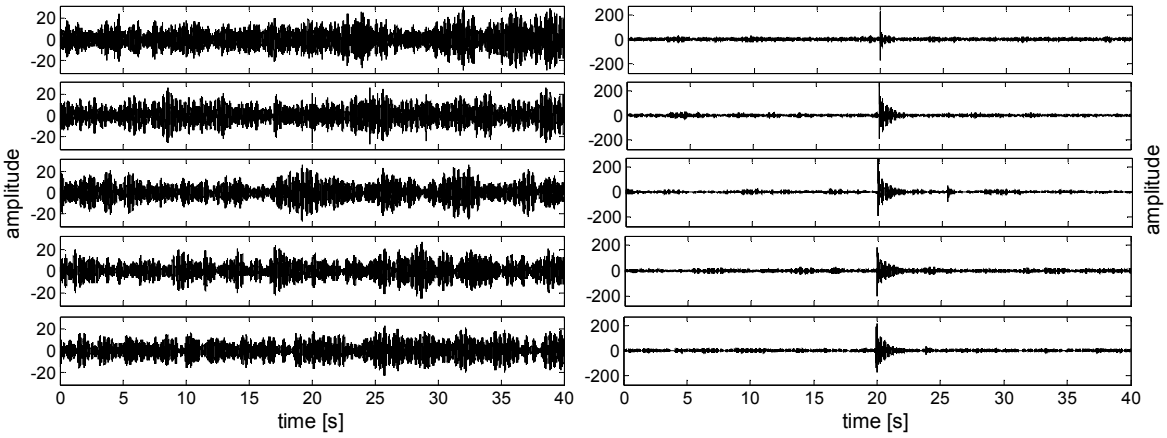

Figure 8. Recorded accelerations at mid-span of the bridge for each of the excitations in Fig. 7. Left: removed mass cases, right: added mass cases.

Based on conventional Fourier analyses of the response of the bridge (with and without added mass) to white noise excitation, the two first natural frequencies of vibration were identified (Fig. 9). For the bridge without added mass, these frequencies were 21.2 Hz and 24 Hz. When the mass is added, these frequencies change to 21.8 Hz and 24.5 Hz. That is, the induced change in frequency is below 3%. The challenge to the time-frequency signal processing analyses is to identify these changes and the time at which they occur.

When the HHT was applied to the raw recorded accelerations, the IMFs extracted exhibited serious mode mixing and identification of the instant frequencies was not possible. An ensemble of EMD

results from different noise added signals (EEMD, Wu and Huang 2009) was also explored obtaining no significant improvements. The results obtained are not presented here due to space constrains. Improved results were obtained when the signal was filtered previous to the application of the HHT. A 10^{th} order Butterworth filter was used to remove frequency contents above 26 Hz and below 19 Hz (Fig. 10). The extracted IMFs for the 30 Hz removed mass case are displayed in Fig. 11. Instant frequencies results are displayed in Fig. 12 for the 30 Hz and 100 Hz removed mass cases; the displayed frequencies (dotted lines) were averaged over a 2 seconds window. It is seen that although the two modes were separated, the resolution at which the frequencies of vibration are estimated does not allow a robust identification of the changes occurring in the system. Similar results were obtained for all the other cases.

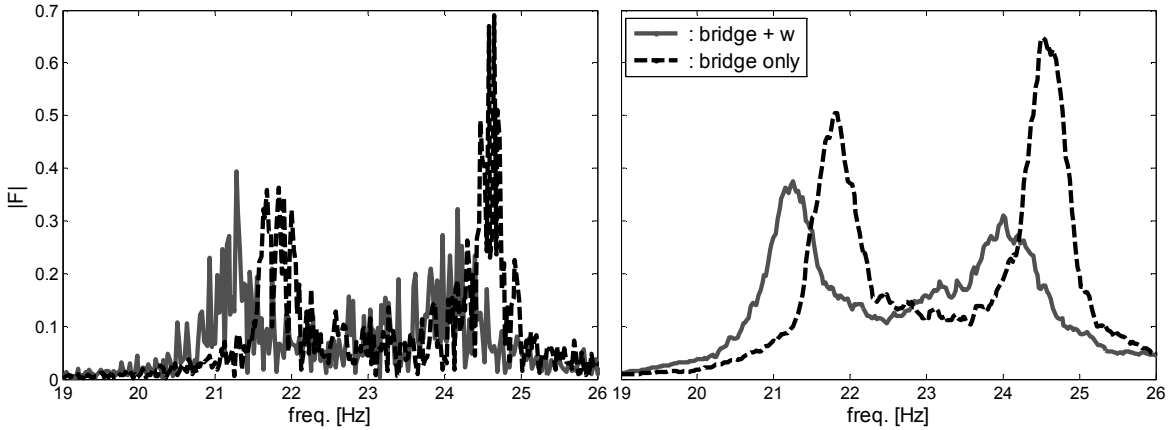

Figure 9. Frequency content of the bridge response with and without added weight. Figure on the right is a smoothed version of the Fourier spectra on the left figure.

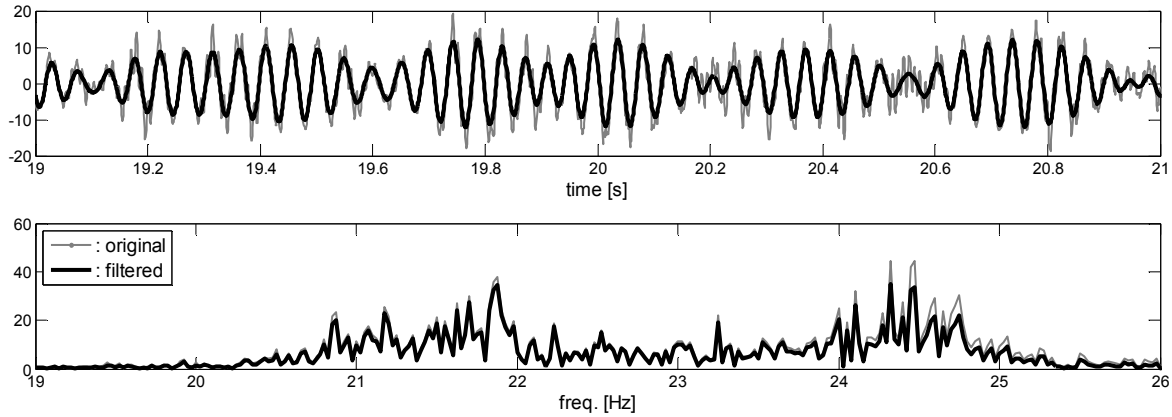

Figure 10. The signal and its Fourier spectrum before and after being filtered.

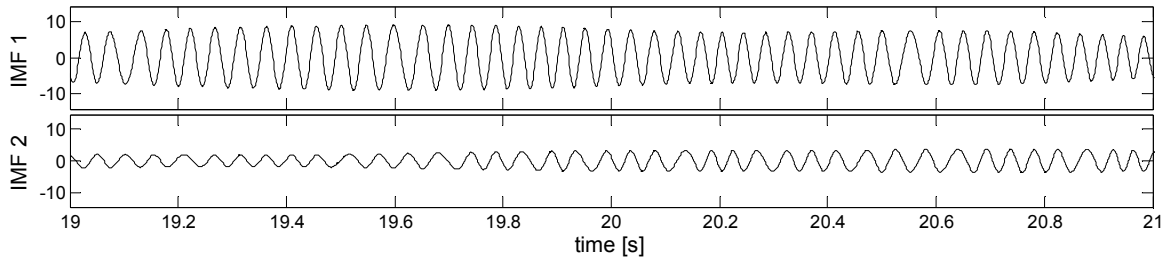

Figure 11. Extracted IMFs via EMD for the 30 Hz removed mass case

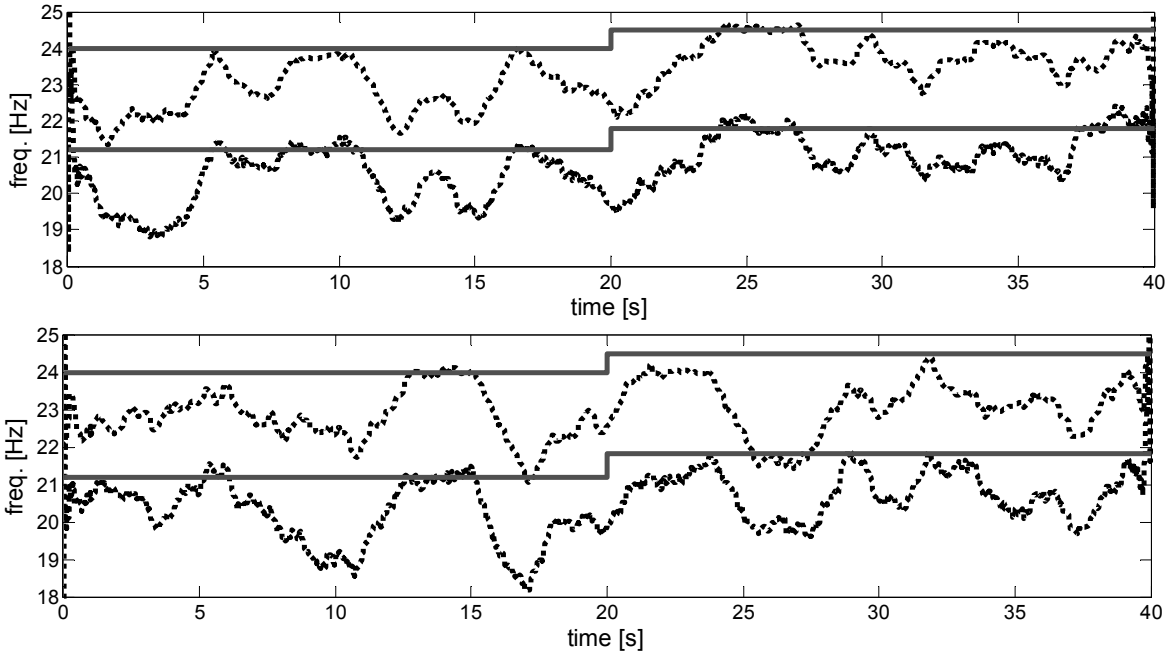

Figure 12. Instant frequencies via HT of the extracted IMFs (dotted lines) and target frequencies (continuous lines). Top: 30 Hz removed mass case, bottom: 100 Hz removed mass case

The results obtained for the CWT analyses at the low and high frequency ranges are displayed for selected cases in Figs. 13 to 16. In these figures the bottom plots present the results of the low frequency analyses, the dotted lines represent the identified horizontal ridges (instant frequencies) and the continuous lines indicate the target values. The ridges can be extracted by a variety of techniques (e.g. Carmona et al 1997); in this work we used the algorithm developed by Jianfeng Lu (Daubuchies et al. 2011). This is a dynamic algorithm that maximizes a functional of the energy of the curve being extracted that penalizes variation. There is a user-defined parameter ($\lambda>0$) that determines the "smoothness" of the resulting curve estimate, we used $\lambda=10\text{^}7$ for all the examples in this work. The top plots present the results for the high frequency analysis [80-512 Hz]. The red dots identify the time at which the maximum wavelet coefficient is reached for each of the frequencies analyzed, this can be think of a "vertical ridge."

From Figs. 13 to 16 it is seen that better results are obtained when the excitation load has limited high frequency content. This is evident when comparing the results obtained for the removed mass cases with white noises excitations with frequency content limited at 30 Hz and 100 Hz (Figs. 13 and 14, respectively). While the difference in the accuracy in which the instant frequencies were estimated may not be significant, the identification of the discontinuity (frequency shift instant) from the high frequency analysis is more stable in the 30Hz case. For the added mass case (Figs. 15 and 16) the quality of the high frequency results is similar for both cases (30 Hz and 100 Hz); however, notice that for the added mass case the discontinuity was evident even from a quick inspection of the acceleration response (Fig. 8).

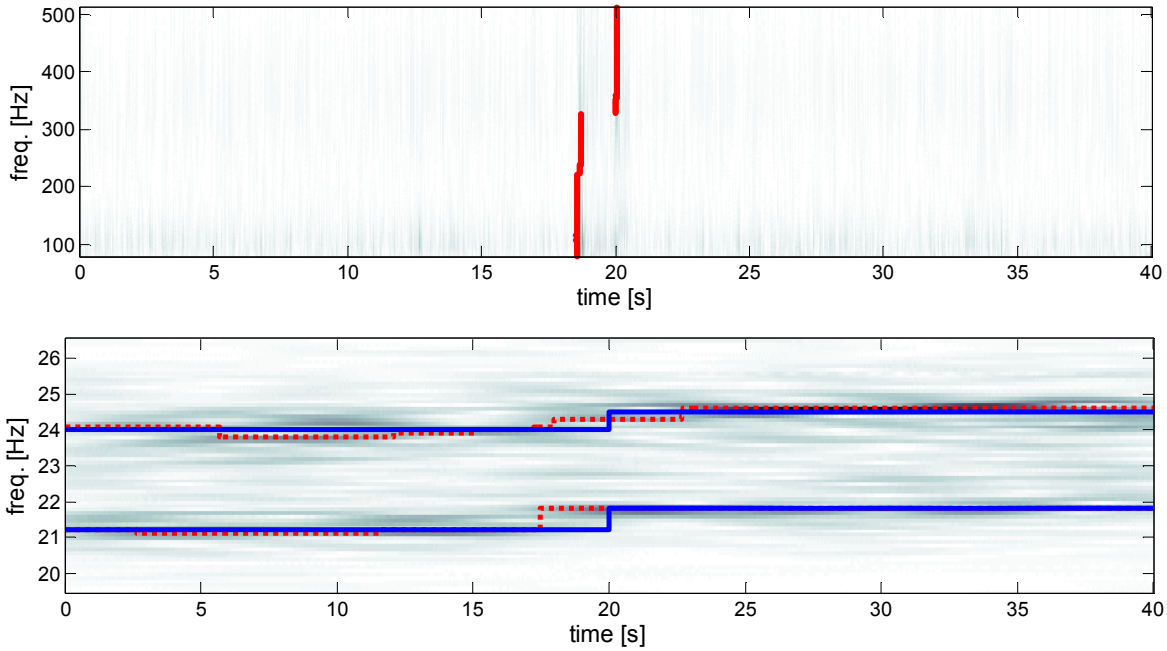

Figure 13. High (top) and low (bottom) frequency wavelet analysis for the 30 Hz removed mass case.

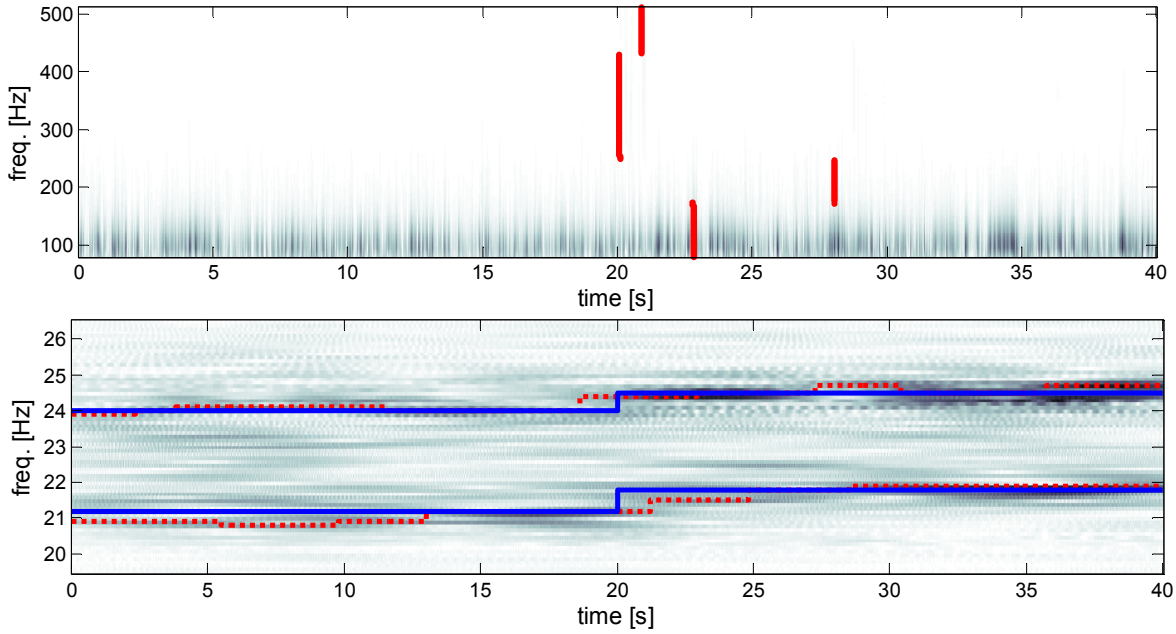

Figure 14. High (top) and low (bottom) frequency wavelet analysis for the 100 Hz removed mass case.

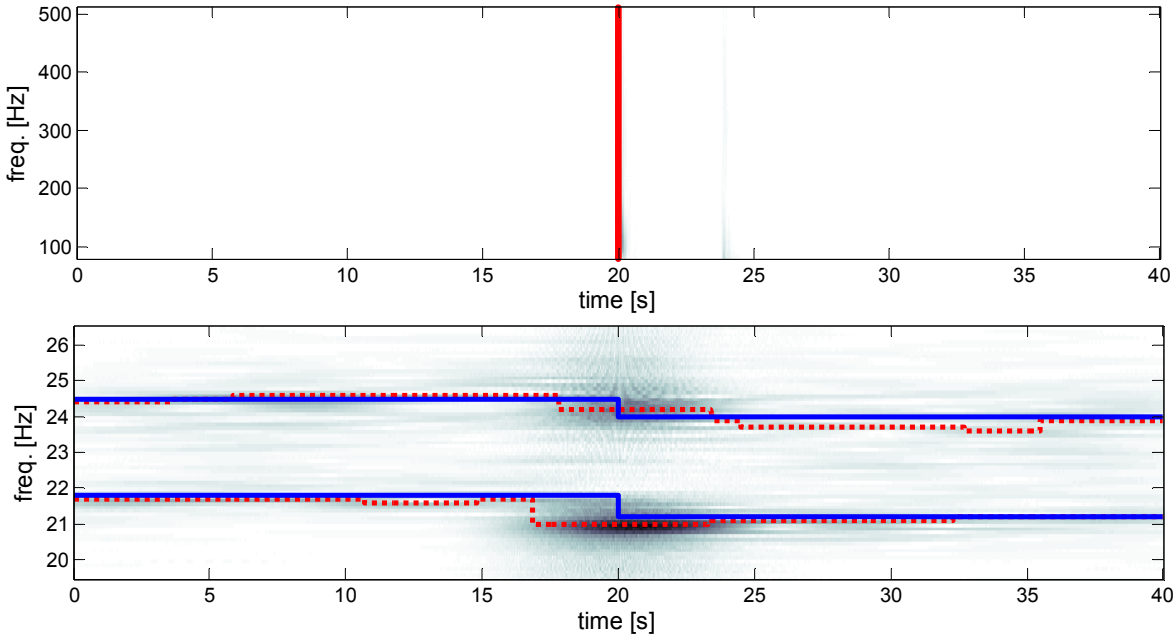

Figure 15. High (top) and low (bottom) frequency wavelet analysis for the 30 Hz added mass case.

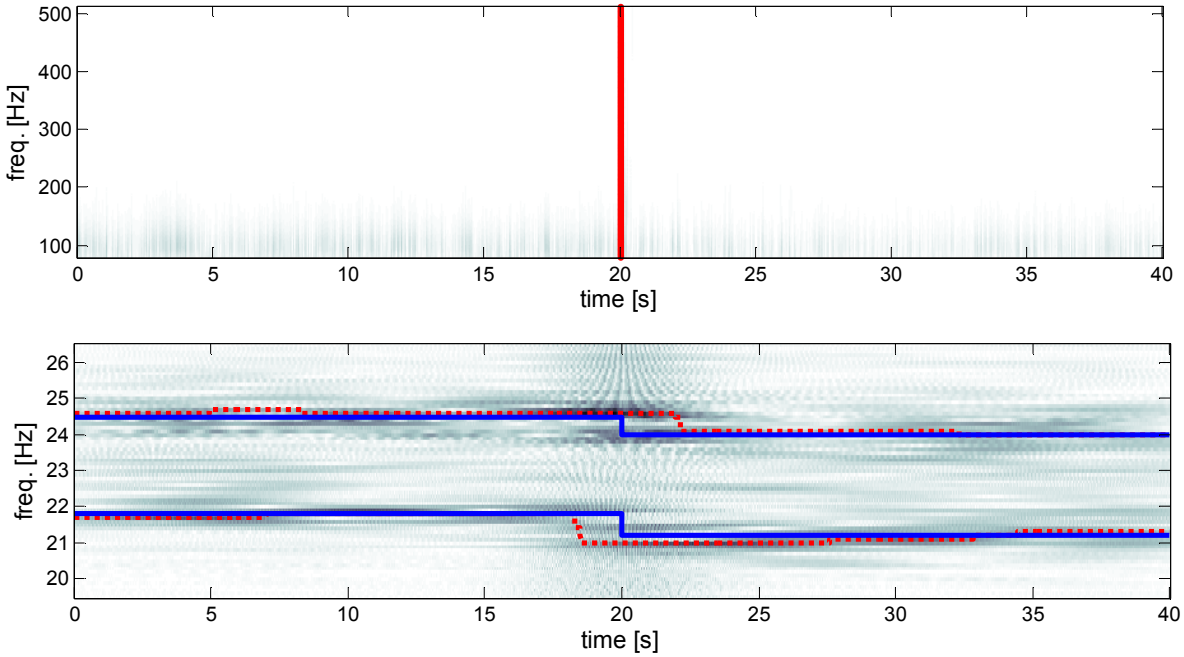

Figure 16. High (top) and low (bottom) frequency wavelet analysis for the 100 Hz added mass case.

5. CONCLUSIONS

HHT and CWT based identification approaches exhibited satisfactory results when evaluated based on a simplified artificially generated signal. Nevertheless, when evaluated under more realistic conditions using vibrational data from a simply supported single-span steel bridge laboratory model, the CWT approach offered better results. The HHT approach was able to separate the first two modal responses in all the cases evaluated, however it required the signal to be pre-filtered, and still the precision at

which the frequencies where estimated did not allow a robust identification of the changes undergone by the system. On the other hand, through the implementation of low and high frequency analyses via CWT, it was possible to identify the frequencies shifts in the system and the time instant at which they occurred.

The results obtained support what has been identified in the past based on numerical simulations (Velazquez and Montejo 2011, Montejo 2011), damage detection methodologies based on the direct examination of the structural response via Wavelet Transforms can be limited by the frequency content of the excitation. Better results are obtained when the high frequency content of the excitation is limited. However, as the high frequency content of the excitation increases, the results obtained after a high frequency analysis may include not only spikes due to structural damage but also anomalies proper of the excitation.

ACKNOWLEDGEMENT

This research was performed under an appointment to the U.S. Department of Homeland Security (DHS) Summer Research Team Program for Minority Serving Institutions, administered by the Oak Ridge Institute for Science and Education (ORISE) through an interagency agreement between the U.S. Department of Energy (DOE) and DHS. ORISE is managed by Oak Ridge Associated Universities (ORAU) under DOE contract number DE-AC05-06OR23100. All opinions expressed in this paper are the author's and do not necessarily reflect the policies and views of DHS, DOE or ORAU/ORISE. Additional support was received from the Puerto Rico Strong Motion Program at the Civil Engineering Department of the University of Puerto Rico at Mayaguez. This support is gratefully acknowledged.

REFERENCES

Carmona, R.A., Hwang, W.L. and Torresani, B. (1997). Characterization of signals by the ridges of their wavelet transforms. *IEEE Transactions on Signal Processing* **54:10**, 2586-2590.

Daubuchies, I., Lu, J. and Wu, H.T. (2011). Synchrosqueezed wavelet transforms: An empirical mode decomposition-like tool. *Applied and Computational Harmonic Analysis* **30**, 243-261.

Feldman, M. (2006). Time varying vibration decomposition and analysis based on the Hilbert transform. *Journal of Sound and Vibration* **295**, 518–530.

Gabor, D. (1946). Theory of communication. *Proceedings of the IEEE* **93(III)**, 429-457

Grossman, A. and Morlet, J. (1990). Decompositions of functions into wavelets of constant shape and related transforms. *Mathematics and Physics – Lecture on Recent Results*, World Scientific, Singapore, 135-65.

Huang, N.E., Shen, Z., Long, S.R., Wu, M.C., Shih, H.H., Zheng, Q., Yen, N.C., Tung, C.C. and Liu, H.H. (1998). The empirical mode decomposition and the Hilbert spectrum for nonlinear and non-stationary time series analysis. *Philosophical Transactions of the Royal Society* **A 454**, 903-995.

Montejo, L.A. (2011). Signal processing based damage detection in structures subjected to random excitations. *Structural Engineering and Mechanics* **4(6)**, 745-762

Rilling, G., Flandrin, P. and Gonçalvès, P. (2003). On empirical mode decomposition and its algorithms. *IEEE-EURASIP Workshop on Nonlinear Signal and Image Processing NSIP-03*.

Velazquez, L.R and Montejo, L.A. (2011). Numerical evaluation of wavelet based detection methodologies applied to RC members", *5th International Conference on Structural Health Monitoring of Intelligent Infrastructure* (SHMII-5), Cancún, México

Wu, Z. and Huang, N.E. (2009). Ensemble empirical mode decomposition: A noise assisted data analysis method. *Advances in Adaptive Data Analysis* **1:1**, 1–41.

Yan, B. and Miyamoto, A. (2006). A comparative study of modal parameter identification based on Wavelet and Hilbert–Huang transforms. *Computer-Aided Civil and Infrastructure Engineering* **21**, 9-23.